Visualizing Topography by *Openness*: A New Application of Image Processing to Digital Elevation Models

Ryuzo Yokoyama, Michio Shirasawa, and Richard J. Pike

Abstract

A new parameter, here termed openness, expressing the degree of dominance or enclosure of a location on an irregular surface, is developed to visualize topographic character. Openness is an angular measure of the relation between surface relief and horizontal distance. For angles less than 90°, it is equivalent to the internal angle of a cone, its apex at a DEM location, constrained by neighboring elevations within a specified radial distance. Openness incorporates the terrain line-of-sight, or viewshed, concept and is calculated from multiple zenith and nadir angles—here along eight azimuths. Openness has two viewer perspectives. Positive values, expressing openness above the surface, are high for convex forms, whereas negative values describe this attribute below the surface and are high for concave forms. Openness values are mapped by gray-scale tones. The emphasis of terrain convexity and concavity in openness maps facilitates the interpretation of landforms on the Earth's surface and its seafloor, and on the planets, as well as features on any irregular surface—such as those generated by industrial procedures.

Introduction

Relief maps and the parametric characterization of topography are essential to the interpretation of the land surface. Hillshaded maps initially were drafted by landscape artists, but map precision and reproducibility were limited by the manual technique and its requisite cartographic skill (Raisz, 1931; Imhof, 1965; Alpha and Winter, 1971). The advent of the electronic computer and the digital elevation model (DEM) overcame these restrictions, and machine-made shaded-relief maps now are widely used to display topography (Yoeli, 1967; Horn and Brooks, 1989; Thelin and Pike, 1991; Vigil *et al.*, 2000). The technique is not without drawbacks of its own. Because a directional light source is required, for example, ridges and valleys intersecting that source are shown clearly while features parallel to the source can be difficult to identify. Attempts to mitigate this problem by multiple light sources have been only partially successful (Mark, 1992; Moore and Mark, 1992; Riehle *et al.*, 1997).

Other types of neighborhood operations centered on DEM grid points yield digital maps that display or extract topographic features (Tobler, 1969; Peucker and Douglas, 1975;

Weibel and Heller, 1991; Blaszczynski 1997; Guth, 2001). Terrain slope, curvature in both the *XY* and *Z* domains, relative relief, and slope azimuth are among the measures most commonly mapped from DEMs (Evans, 1972; Pike, 1988). Algorithms that implement the much-used DEM-to-watershed transformation, now an essential tool for hydrologic and geomorphic modeling, incorporate several such measures (Jenson and Domingue, 1988; ESRI, 1992). Like automated relief-shading, however, all of these parameters are sensitive to the vagaries inherent in gridded height data (Carter, 1992). In particular, slope maps computed from DEMs commonly have an unsatisfactory wormlike appearance that reflects the method of contour gridding and obscures the true configuration of the land surface.

In this paper, we introduce a new concept of surface representation, provisionally termed *openness* for want of a better name. It is a novel method for digital terrain modeling—actually an image-processing technique—by which values of surface openness are calculated from a DEM, displayed in map form, and used to visualize landscapes. The resulting maps of openness superficially resemble digital images of shaded relief or slope angle, but emphasize dominant surface concavities and convexities. Values of openness require no light source, thus removing one limitation of relief shading, and are less affected by the DEM noise that afflicts most other parameters. After describing the technique, we present several maps of surface openness and discuss how they may be applied to the analysis and interpretation of topography.

Zenith and Nadir Angles

Before defining topographic openness, we must establish some angular relations between the point locations along individual DEM-derived profiles, and do this for viewer perspectives both above and below the surface. The first quantity to be extracted from these relations is elevation angle θ.

Figure 1 shows a sample of terrain heights in a DEM arrayed north-south and east-west at a constant spacing M, projected in Universal Transverse Mercator (UTM) coordinates, and centered on a point of interest (double circle). Each point in the DEM is described by (i, j, H) where i and j are column and row numbers and H is elevation. Figure 2 defines the geometric relation in profile between any two points $\mathbf{A}(i_A, j_A, H_A)$ and $\mathbf{B}(i_B, j_B, H_B)$ in the DEM, here showing a case where $H_A < H_B$. Horizontal distance P between $\mathbf{A}$ and $\mathbf{B}$ is given by

R. Yokoyama and M. Shirasawa are with the Department of Computer and Information Science, Faculty of Engineering, Iwate University, 4-3-5, Ueda, Morioka, Iwate, 020-8551 Japan (yokoyama@cis.iwate-u.ac.jp).

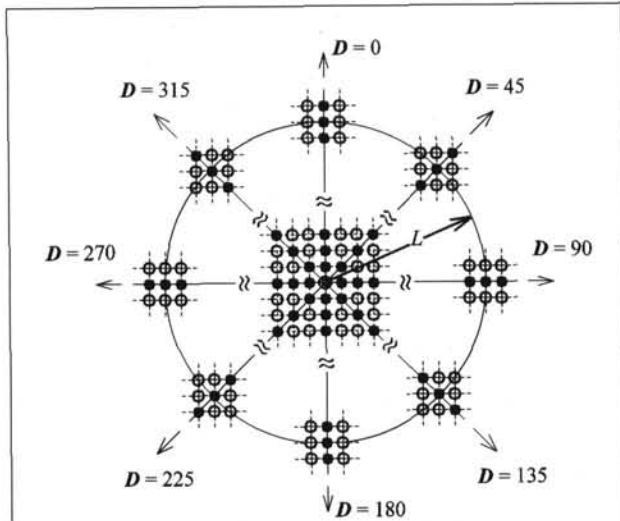R.J. Pike is with the U.S. Geological Survey, M/S 975, 345 Middlefield Road, Menlo Park, CA 94025.

Figure 1. Selected elevations arrayed in a DEM. Double circle is origin point for the calculation of openness; solid points are heights outward from that point along each of the eight azimuths; azimuth angle **D** is measured clockwise from north. **L** is radial limit of the calculation.
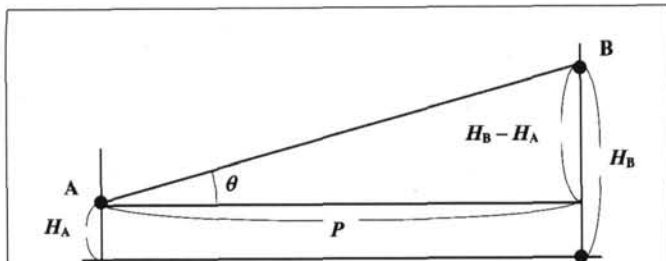

Figure 2. Elevation angle θ between two points on a DEM. Terrain height **A(i_A, j_A, H_A)** is at the origin of the calculation; height **B(i_B, j_B, H_B)** lies at some horizontal distance **P** on the DEM. θ is assumed to be positive for $H_A < H_B$, and negative for $H_B < H_A$.

$$P = M \sqrt{(i_A - i_B)^2 + (j_A - j_B)^2} \tag{1}$$

and the elevation angle θ of line **AB** is

$$\theta = \tan^{-1}\left\{\frac{(H_B - H_A)}{P}\right\}. \tag{2}$$

Angle θ is positive when $H_A < H_B$ and *negative* when $H_B < H_A$. A general treatment of **P** and θ would incorporate Earth's curvature, but this can be neglected because the calculation requires only small patches of terrain and thus short horizontal distances. Angle θ enables us to identify a **D - L** set.

Definition 1: A **D - L** set for a DEM grid point is the set of all elevation angles (θ) between that point and each of the grid points (filled circles in Figure 1) located on a profile along an azimuth **D** and within radial distance **L**. The largest θ in the **D - L** set, shown in Figure 3, is required to calculate elevation angles. By expressing the **D - L** set as $_D S_L$, we introduce two quantities,

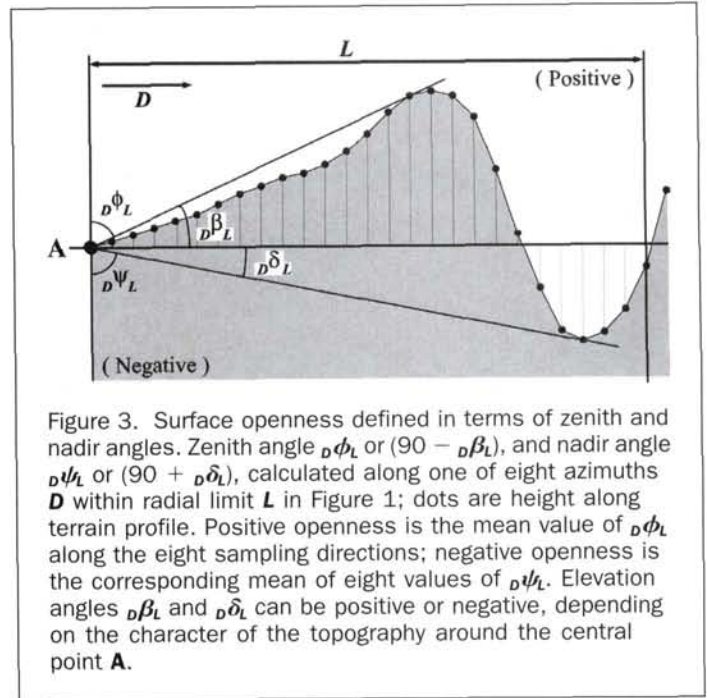
Figure 3. Surface openness defined in terms of zenith and nadir angles. Zenith angle $_D\phi_L$ or $(90 - _D\beta_L)$, and nadir angle $_D\psi_L$ or $(90 + _D\delta_L)$, calculated along one of eight azimuths **D** within radial limit **L** in Figure 1; dots are height along terrain profile. Positive openness is the mean value of $_D\phi_L$ along the eight sampling directions; negative openness is the corresponding mean of eight values of $_D\psi_L$. Elevation angles $_D\beta_L$ and $_D\delta_L$ can be positive or negative, depending on the character of the topography around the central point **A**.

$_D\beta_L$: the maximum elevation angle in the $_D S_L$

and

$_D\delta_L$: the minimum elevation angle in the $_D S_L$.

These angles, the minimum angles of elevation or depression, respectively, for which the line-of-sight is unobstructed out to a specified range (here **L**), are the *mask angles* of the military tactician (Wood, 1963; Anon., 1990). These two angles, which also are involved in the calculation of terrain viewsheds (Lee, 1994, Fisher, 1996), enable us to define the next quantity.

Definition 2: The *zenith angle* at a DEM grid point along azimuth **D** within radial distance **L** is

$$_D\phi_L = 90 - _D\beta_L \tag{3}$$

and the *nadir angle*

$$_D\psi_L = 90 + _D\delta_L \tag{4}$$

As illustrated in Figure 3, the zenith angle $_D\phi_L$ is the maximum vertical angle subtended by a selected grid point and any of the points viewed from *above* the surface along a chosen azimuth **D** up to distance **L**. The corresponding nadir angle $_D\Psi_L$ for that point is the maximum angle subtended by the chosen point and any other point viewed from *below* the surface along azimuth **D** within **L**. Like terrain mask-angles, $_D\phi_L$ and $_D\Psi_L$ thus depend both upon the configuration of the surface surrounding the point of interest and upon the specified range **L** within which points are considered. Moreover, because $_D S_L$ computed within increasingly large distances **L** includes more grid points, but not necessarily a commensurate increase in terrain relief, both $_D\phi_L$ and $_D\Psi_L$ tend to diminish with increasing **L**.

Openness

We obtain surface openness by calculating either zenith or nadir angles for all eight compass directions from the central point **A** (double circled in Figure 1) and taking the mean.

Definition 3: *Positive openness* Φ_L at a location on a surface within the distance of L on the DEM is

$$\Phi_L = (_0\phi_L + {}_{45}\phi_L + \ldots + {}_{315}\phi_L)/8 \qquad (5)$$

and *negative openness* Ψ_L within a distance L is

$$\Psi_L = (_0\psi_L + {}_{45}\psi_L + \ldots + {}_{315}\psi_L)/8. \qquad (6)$$

Positive openness at a DEM grid point A is the average of *zenith* angles subtended by A and the optimal point (that yielding the highest angle) viewed *above* the surface along each of the eight azimuths D_{0-315}—up to the specified distance L (Figure 3). Similarly, *negative* openness averages the eight *nadir* angles subtended by point A and the optimal point viewed *below* the surface along azimuths D_{0-315} within L. To forestall possible confusion, we note that values of Φ_L and Ψ_L always take the positive sign. Openness is designated "positive" and "negative" to avoid the awkward terminology cited in the next paragraph. We adopt this "positive"/"negative" convention in the same sense as has been used to express terrain-slope curvature (Pike, 1988), which also takes only positive values (positive curvature is convex-upward; negative curvature is concave-upward).

Positive, or "above-ground," openness Φ_L at a grid point is constrained by surrounding topography and thus is an angular estimate of the 360° horizontal extent of area around the point. We originally conceptualized the measure as "openness of the terrain to the sky." Its negative counterpart, "below-ground" openness Ψ_L—less helpfully verbalized as openness *per se*—is the corresponding angular measure of 360° spatial extent around the central grid point. Figure 4, which shows these two measures schematically for angles < 90°, represents openness as the largest right cone of specified base diameter $2L$ that can be fit to a point on a DEM. Comparable representations of Φ_L and $\Psi_L > 90°$ are impossible-to-illustrate constructs in topology (e.g., Barr, 1964) that are better rendered in two dimensions, as in Figures 5A and 5D. Figure 4 is a simplification of the true figure of merit, because the base of the conical figure actually fit to the terrain rarely will be a perfect circle of diameter $2L$. As shown in Figure 6, the base will have an irregular, commonly elongate and eccentric, form that necessarily varies with the elevation angles determined along the eight azimuths.

Like its constituent individual zenith $(_D\phi_L)$ and nadir $(_D\psi_L)$ angles, the corresponding mean values of openness Φ_L and Ψ_L also are constrained to decrease with increasing range L. Accordingly, the choice of L will emphasize topography at different length scales. Larger values of L will highlight larger features, and smaller L smaller forms.
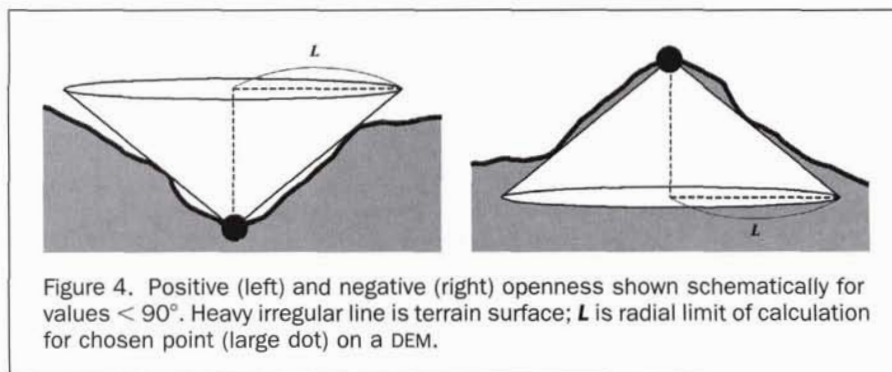
Discussion

Openness expresses a topographic attribute that possibly is captured by no other measure or combination of them,

although this remains to be tested against parameters that describe terrain fabric (Pike *et al.*, 1989; Guth, 2001). The characteristic appears to be the degree of geometric "dominance" of one location on a surface by another. This parameter expresses two configurations commonly encountered in the landscape: command of an expanse of terrain by one or several elevated relief features (positive openness Φ_L), and the degree of "enclosure" of a lower location by elevated surroundings (negative openness Ψ_L). As such, openness is sensitive to the local relief: distance conditions that express much of an area's topographic distinctiveness (Pike *et al.*, 1989).

The range of contrasts is illustrated by profiles of a hilltop and a closed depression along the azimuth D_{90}-D_{270} (Figure 5). If the center point of an openness calculation is on a summit rising above its surroundings and flanked by steep slopes, the resulting values of $_{90}\phi_L$ and $_{270}\phi_L$ will exceed 90° (Figure 5A), as will positive openness Φ_L, which is the average of eight values of $_D\phi_L$. Summits and ridge lines thus will appear on a plot of Φ_L as, respectively, compact and linear groupings of high-scoring cells. Commensurately, a negative-openness calculation at the same location (Figure 5B) would yield low values of $_{90}\psi_L$ and $_{270}\psi_L$, < 90°, and summits and ridge lines on a plot of Ψ_L will be groups of low-scoring cells. Topographic features that result in neither high nor low values of Φ_L and Ψ_L yield groupings of intermediate-scoring cells. Taking the inverse example, if the center point of an openness calculation lies within a depression surrounded by steep slopes (Figure 5C), the resulting value of positive openness Φ_L will be less than 90 degrees. Topographic lows, therefore, will appear on maps of Φ_L as groups of low-scoring cells. However, that same depression will generate a high value of negative openness $\Psi_L > 90°$ (Figure 5D). Topographic depressions and valley lines thus will show up on a (L plot as clusters and strings of high-scoring cells.

The closed-depression example, which is the approximate inverse of the summit example, raises an intriguing point. Figure 5 would at first appear to show that negative openness is redundant: that simply subtracting Φ_L from 180° would be equivalent to Ψ_L, but this is not so. The two quantities differ substantially, due to irregularity of the ground surface surrounding point A. It is for this reason that negative openness Ψ_L emphasizes concave features (Figure 5D) more crisply in gray-tone images (Figures 7 through 13 below) than does $180° - \Phi_L$ (Figure 5C). Otherwise, $180° - \Phi_L$ would suffice to capture depressions and valleys and there would be no need for Ψ_L.

The correspondence of openness to terrain configuration is illustrated in Figure 6 by octagonal plots that compare *zenith* and *nadir* angles, along the eight azimuths, for nine test surfaces. Among these simple models are all the important elements of topography—plain, slope, summit, depression, ridge, valley, and saddle (Maxwell, 1870). Depending on shape of the ground, angular values of $_D\phi_L$ and $_D\psi_L$ increase with distance outward from the center of each figure, up to range L. Openness is equivalent to the area of the octagon projected at L. Because
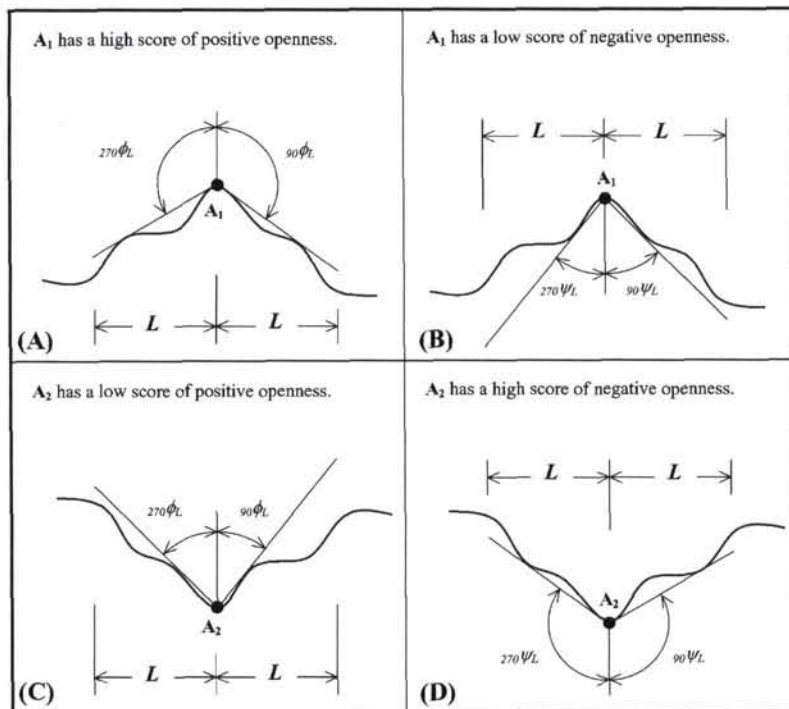

Figure 4. Positive (left) and negative (right) openness shown schematically for values < 90°. Heavy irregular line is terrain surface; L is radial limit of calculation for chosen point (large dot) on a DEM.

A₁ has a high score of positive openness.	A₁ has a low score of negative openness.
(A)	(B)
A₂ has a low score of positive openness.	A₂ has a high score of negative openness.
(C)	(D)

Figure 5. High and low values of positive Φ_L and negative Ψ_L surface openness, illustrated. Profiles of a hilltop and closed depression along azimuth D_{90}-D_{270} (**E-W**). Values of $_{90}\phi_L$ and $_{270}\phi_L$ for point A_1 each $> 90°$ in (A), but values of $_{90}\psi_L$ and $_{270}\psi_L < 90°$ in (B). Because Φ_L and Ψ_L are means of $_D\phi_L$ and $_D\psi_L$ along eight azimuths, Φ_L at $A_1 > 90°$ and $\Psi_L < 90°$. Similarly, $_{90}\phi_L$ and $_{270}\phi_L$ for point A_2 each $< 90°$ in (C), but those of $_{90}\psi_L$ and $_{270}\psi_L > 90°$ in (D), thus Φ_L at $A_2 < 90°$ and $\Psi_L > 90°$. None of these angles is larger 180°.

features in natural terrain are complex composites of these basic elements, the set of eight angles that comprise openness will vary considerably with location of the point of origin and character of the surrounding topography. A grid point in highly irregular terrain thus will generate a variety of constituent angles and a correspondingly distorted octagonal pattern. The angular plots in Figure 6 constitute a kind of geometric signature of topographic form; openness also could be part of a more complex, multivariate signature (Pike, 1988).

Examples and Applications

While we defer the application of corresponding values of openness as an analytical parameter—for example, as a constituent of a geometric signature—to a later experiment, in this paper we exemplify the visualization counterpart of terrain modeling by several maps of surface openness. These few selections represent a variety of terrains, map scales, **L**-values, and DEM sources and resolutions. Not all possible combinations of these applications are shown. In order to highlight both terrain convexities and concavities, for example, values of positive openness and negative openness must be compiled as separate maps of the same area. Also, separate openness maps of the same area can be computed for different values of **L**, to emphasize fine- or coarse-scale features.

As in mapping elevation, slope, and shaded relief calculated from DEMs, tones of gray are assigned to values of openness within a range that produces an image with optimal detail and contrast. The convention adopted for our images is that customarily followed for elevation and slope: high values of

openness are represented by light tones and low values by dark tones. Accordingly, images of positive openness Φ_L, which are designed to highlight topographic convexities, show ridges as bright lines and rivers and other elongate concavities as dark lines, whereas maps of negative openness Ψ_L emphasize drainages (light tones) at the expense of mountains and other convex-overall features (dark tones). Intermediate values of both parameters yield gray tones. Although we experimented with reversing this tonal convention, we chose the standard scheme on aesthetic and intuitive grounds—the resulting images simply look more pleasing to the eye and seem easier to interpret. Mapping openness values carries some perceptual consequences. While openness images superficially resemble raster-based maps of elevation, shaded relief, or slope, their appearance can be deceiving at first. Individuals familiar with the more conventional types of digital maps may require some acclimation to openness images before viewing them becomes intuitive.

Maps of positive openness in Figures 7 and 8, computed at different values of **L**, illustrate various features of stratovolcanoes on the main Japanese island of Honshu (Yoshikawa et al., 1981, p. 81–87). Landforms in the vicinity of Mt. Fuji in south-central Honshu (Figure 7) that are easily recognized from openness textures include aligned low hummocky hills formed in flank eruptions prior to 1707 (light-toned area, center). Steep ridges in much of the image appear as bright thin lines; old lava flows on Fuji and the more gently sloping ridges on the eroded Mt. Ashitaka volcano and Hakone caldera to the Southeast are less distinct. The area around Mt. Chokai in

Figure 6. Variation in surface openness. Differing values of the eight zenith angles $_D\phi_L$ and nadir angles $_D\psi_L$, at a DEM grid point (black dot), for nine simple terrains. Positive and negative openness Φ_L and Ψ_L are proportional to the area enclosed by the octagonal plots of $_D\phi_L$ and $_D\psi_L$, respectively. Evenly-spaced numbers 1 through 7 along azimuths are for comparison purposes and do not correspond to actual angles; range **L** for all calculations = 7.
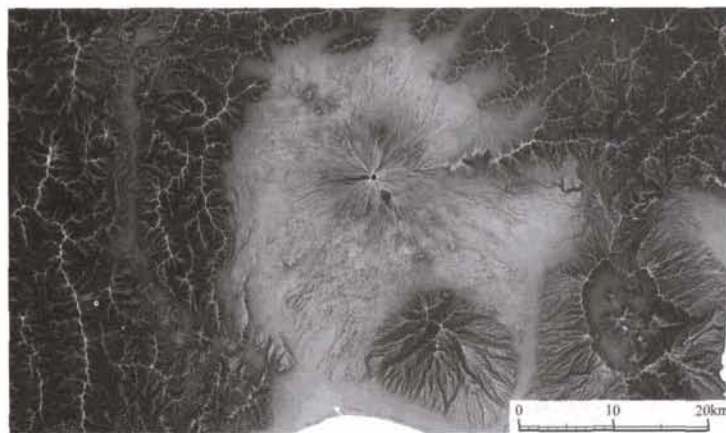
Figure 7. Positive openness (*L* = 5 km) for the Mt. Fuji area, southern Honshu (N35:06:24 - N35:31:42, E138:18:07 - E139:09:16) computed from a 50-m DEM of the Geographical Survey Institute of Japan (GSIJ).
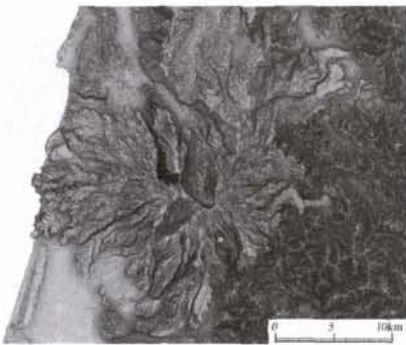
Figure 8. Positive openness (*L* = 1 km) for Mt. Chokai, northern Honshu (N38:43:41 - N38:59:32, E139:44:49 - E140:14:56) computed from a 10-m DEM from the Hokkaido Map Company (HMC).

northwest Honshu (Figure 8), rendered at one-fifth the value of *L* in Figure 7, is more detailed and also differs in morphology from the area around Mt. Fuji. The recent growth process of the volcano, clearly evident in the lobate form of its many fresh lava flows, is well illustrated by positive openness.

Figures 9 and 10 contrast two non-volcanic terrains in Japan in maps of negative openness that emphasize topographic concavities at very different values of *L*. The Tohkamachi area (Figure 9), located in the upper reaches of the Shinano River in north-central Honshu, exemplifies variation in the patterns of valleys as well as in the layers of sediment in the main valley. Figure 10 shows the Tohno area, east of Mt. Chokai. The distinctly reticular structure of this terrain, at one-tenth the *L* used to compute Figure 9, reflects small stream channels that developed along planes of weakness caused by jointing in the underlying granite bedrock. Because the area is densely vegetated, the macroscopic structure of this joint pattern had remained unknown to geologists and is shown clearly here for the first time (Kanisawa and Yokoyama, 1999). More variety of topographic features can be observed in the openness maps of Japan (Yokoyama, 2001), which were generated from a 50-m interval DEM with *L* = 5 km and printed at a scale of 1:50,000.

Figures 11 and 12, showing positive and negative openness at the same *L*-value for a small area 50 km south of San Francisco in California's coastal Santa Cruz Mountains, are excerpted from two large openness maps of the entire ten-county San Francisco Bay region (not shown). Most of this rough terrain lies within the La Honda 7.5-minute quadrangle, the first topographic map published by the U.S. Geological Survey in which a contour-to-grid technique replaced photogrammetric scanning to create a higher quality 30-m DEM (Pike *et al.*, 1987). The crisp valleys and ridge lines in Figures 11 and 12, respectively, reflect the region's strong contrasts in rock type (Pike *et al.*, 1988) as well as the imprint of recent tectonic uplift and consequent erosion. The steep terrain is subject to chronic debris-flow (landslide) activity during the rainy California winter and thus is thinly populated.

The lofty topography of Tibet and the high-relief Himalaya Range are attracting fresh scientific interest (Fielding *et al.*, 1994; Albright *et al.*, 1998; Zeitler *et al.*, 2001). Figure 13, a negative openness map of this large region, emphasizes the hydrology of the southern Tibetan Plateau and its relation to the Himalayas. The distinctive north-south valleys were carved through the rising mountains by rivers draining the plateau. The contrasting rectangular areas reflect differences in the source and quality of data in the GTOPO30 DEM. This contrast is an important feature of the openness parameter. The large map of negative openness (not shown) containing the California sample in Figures 11 and 12 also revealed an imperfect match between two source DEMs—suggesting that the openness is an excellent tool for performing quality control on regional DEMs mosaicked from several smaller data sets.

Application of openness need not be limited to the portrayal and interpretation of Earth's landscapes. Like shaded-relief mapping, openness mapping is an image-processing technique capable of representing surface features anywhere a DEM exists or can be prepared—Earth's seafloor (Smith and Sandwell, 1997) and surfaces of the solid planets and satellites (Smith *et al.*, 1999). Finally, the technique is not restricted to natural landscapes. Digital terrain modeling has an important micro- and nano-scale counterpart in *surface metrology*, the numerical characterization of industrial surfaces—such as *magnetic tape and disk surfaces and automobile-engine cylinder walls* (Pike, 2000; Pike, 2001). Metrology recently was revolutionized by its ability to create and manipulate square-grid height matrices that are fine-scale analogs of DEMs. Because the
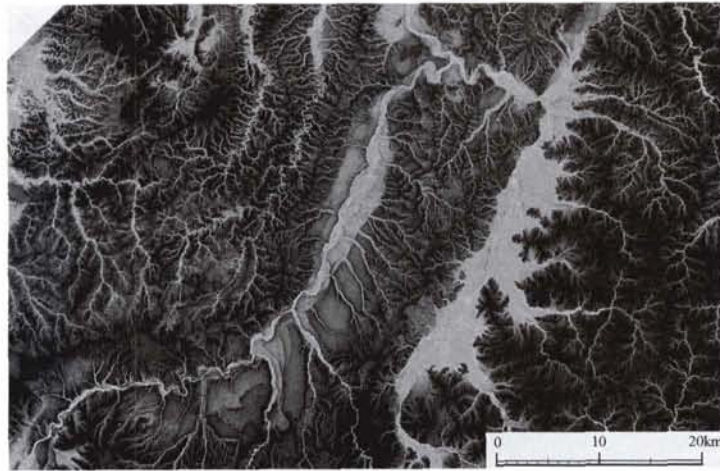
Figure 9. Negative openness (**L** = 5 km) for the Tohka-machi area, central Honshu (N36:54:07 - N37:19:20, E138:21:58-E139:09:05) computed from the 50-m GSIJ DEM.
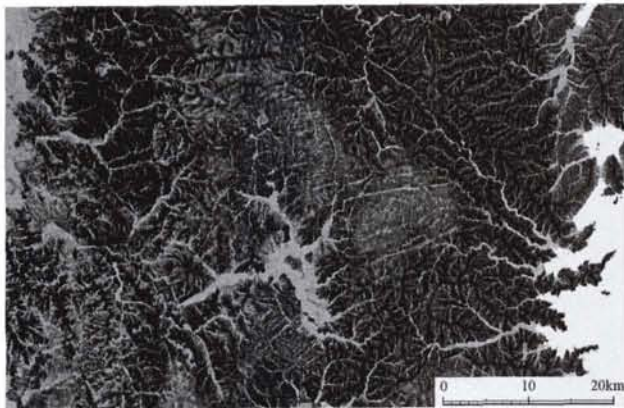

Figure 10. Negative openness (**L** = 500 m) for Tohno area, central Honshu (N39:11:00 - N39:36:41, E141:09:58 - E142:01:06) computed from a 10-m DEM from HMC.

Figure 12. Negative openness (**L** = 500 m) for the area in Figure 11.

Figure 11. Positive openness (**L** = 500 m) for an area south of San Francisco, California (N37:10:03 - N37:17:43, W122:06:01 - W122:22:1) computed from a 30-m DEM of the U.S. Geological Survey (USGS).

surface topography of manufactured components is routinely modeled by the same techniques of parameterization and visualization as used in the Earth sciences, we suggest that the concept of surface openness offers a new tool for metrologic applications as well.

Conclusion

A new image-processing technique generates an angular measure of surface form, here termed *openness*, that visualizes the topographic dominance or enclosure of any location on an irregular surface represented by a DEM. The measure incorporates the terrain line-of-sight (viewshed) principle and is calculated from zenith and nadir angles along eight DEM azimuths. Openness is expressed in two modes. Positive openness emphasizes convex features of topography and negative openness concave features. Values of openness, which are shown as gray-scale maps resembling shaded-relief images, are independent of the position of any light source and less sensitive to noisy DEMs than are other parameters. Different topographic features can be emphasized by tailoring a radial sampling distance to the scale of the selected area. Openness maps not only create new possibilities for geomorphological and geographical
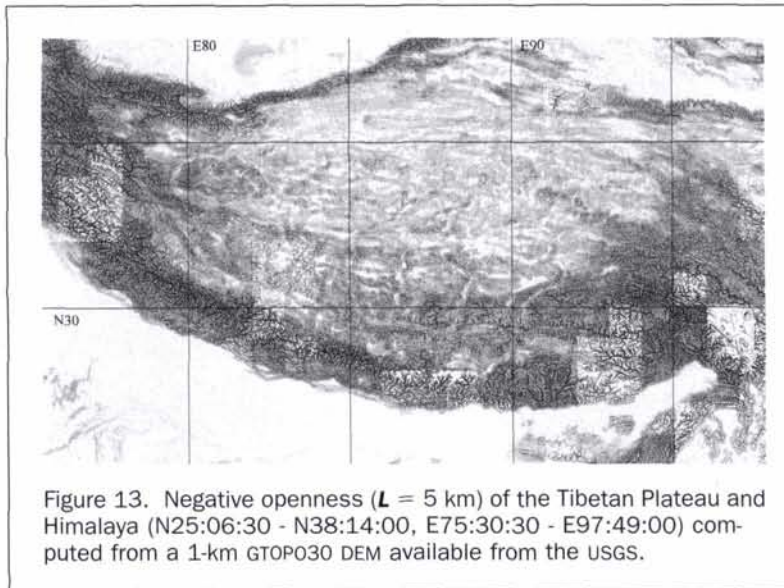
Figure 13. Negative openness (**L** = 5 km) of the Tibetan Plateau and Himalaya (N25:06:30 - N38:14:00, E75:30:30 - E97:49:00) computed from a 1-km GTOPO30 DEM available from the USGS.

interpretation, but also are suited to visualization of the Earth's seafloor, planetary landforms, and features on any irregular surface, including those micro- and nano-landscapes created by manufacturing processes.
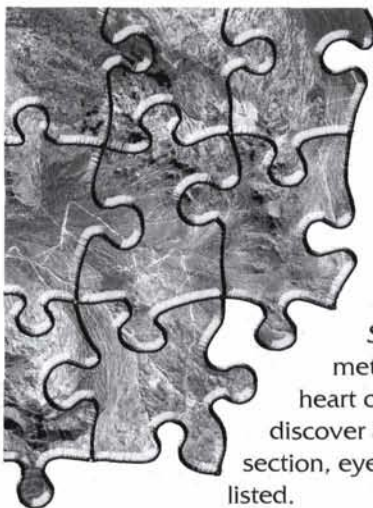
Acknowledgment

References

Albright, T.P., T.H. Painter, D.A. Roberts, J. Shi, J. Dozier, and E. Fielding, 1998. Classification of surface types using SIR-C/X-SAR, Mount Everest Area, Tibet, *Journal of Geophysical Research*, 103(E11):25823–25837.

Alpha, T.R., and R.E. Winter, 1971. Quantitative physiographic method of landform portrayal, *Canadian Cartographer*, 8(2):126–136.

Anonymous, 1990. *Firefinder Mask Considerations, Tactics, Techniques, and Procedures for Field Artillery Target Acquisition*, FM 6-121, Appendix F, Headquarters, Department of the Army, Washington, D.C., 5 p. http://www.adtdl.army.mil/cgi-bin/atdl.dll/fm/6-121/appf.pdf.

Barr, S., 1964. *Experiments in Topology*, Crowell, New York, N.Y., 210 p. (reprinted 1989, Dover Publications, New York, N.Y.)

Blaszczynski, J.S., 1997. Landform characterization with geographic information systems, *Photogrammetric Engineering & Remote Sensing*, 63(2):183–191.

Carter, J.R., 1992. The effect of data precision on the calculation of slope and aspect using gridded DEMs, *Cartographica*, 29(1):22–34.

ESRI, 1992. *Cell-Based Modeling with GRID 6.1, ARC/INFO User's Guide, Supplement—Hydrologic and Distance Modeling Tools*, Environmental Systems Research Institute Inc., Redlands, California, variously paged.

Evans, I.S., 1972. General geomorphometry, derivatives of altitude and descriptive statistics, *Spatial Analysis in Geomorphology* (R.J. Chorley, editor), Harper and Row, New York, N.Y., pp. 17–90.

Fielding, E.J., B.L. Isacks, M. Barazangi, and C.C. Duncan, 1994. How flat is Tibet? *Geology*, 22(2):163–167.

Fisher, P.F., 1996. Extending the applicability of viewsheds in landscape planning, *Photogrammetric Engineering & Remote Sensing*, 62(11):1297–1302.

Guth, P.L., 2001. Quantifying terrain fabric in digital elevation models, *The Environmental Legacy of Military Operations* (J. Ehlen and R.S. Harmon, editors), Geological Society of America Reviews in Engineering Geology, 14, chap. 3 (in-press).

Horn, B.K.P., and M.J. Brooks (editors), 1989. *Shape from Shading*, M.I.T. Press, Cambridge, Massachusetts, 577 p.

Imhof, E., 1965. *Kartographische Geländedarstellung*, Walter de Gruyter, Berlin, Germany, 425 p.

Jenson, S.K., and J.O. Domingue, 1988. Extracting topographic structure from digital elevation data for geographic information systems analysis, *Photogrammetric Engineering & Remote Sensing*, 54(11):1593–1600.

Kanisawa, S., and R. Yokoyama, 1999. Extraction of geologic information from digital elevation map of 50m-mesh—Application of slope and openness maps to the Kitakami Mountains, *Chisitsu News*, (542):31–38 (in Japanese).

Lee, J., 1994. Digital analysis of viewshed inclusion and topographic features on digital elevation models, *Photogrammetric Engineering & Remote Sensing*, 60(4):451–456.

Mark, R.K., 1992. *A Multidirectional, Oblique-Weighted, Shaded-Relief Image of the Island of Hawaii*, U.S. Geological Survey Open-file Report 92-422, U.S. Geological Survey, Reston, Virginia, 3 p.

Maxwell, J.C., 1870. On hills and dales, *The London, Edinburgh, and Dublin Philosophical Magazine and Journal of Science*, 40 (4th Series, July-Dec., No. 269):421–427.

Moore, J.G., and R.K. Mark, 1992. Morphology of the island of Hawaii, *GSA Today*, 2(12):257–259 and 262.

Peucker, T.K., and D.H. Douglas, 1975. Detection of surface-specific points by local parallel processing of discrete terrain elevation data, *Computer Graphics and Image Processing*, 4(4):375–387.

Pike, R.J., 1988. The geometric signature—Quantifying landslide-terrain types from digital elevation models, *Mathematical Geology*, 20(5):491–511.

———, 2000. Nano-metrology and terrain modelling—Convergent practice in surface characterisation, *Tribology International*, 33(9):593–600.

———, 2001. Digital terrain modeling and industrial surface metrology—Converging realms, *The Professional Geographer*, 53(2):263–274.

Pike, R.J., W. Acevedo, and D.H. Card, 1989. Topographic grain automated from digital elevation models, *Proceedings, Ninth International Symposium on Computer-Assisted Cartography*, 02–07 April, Baltimore, Maryland (American Society for Photogrammetry and Remote Sensing—American Congress on Surveying and Mapping), pp. 128–137.

Pike, R.J., W. Acevedo, and G.P. Thelin, 1988. Some topographic ingredients of a geographic information system, *Proceedings, International Geographic Information Systems Symposium*, 15–18 November, Arlington, Virginia (NASA, Washington, D.C.), 2:151–164.

Pike, R.J., G.P. Thelin, and W. Acevedo, 1987. A topographic base for GIS from automated TINs and image-processed DEMs, *Proceedings, GIS '87, Second International Conference, Exhibits, and Workshops on Geographic Information Systems*, 26–30 October, San Francisco, California (American Society for Photogrammetry and Remote Sensing/American Congress on Surveying and Mapping), 1:340–351.

Raisz, E., 1931. The physiographic method of representing scenery on maps, *Geographical Review*, 21(2):297–304.

Riehle, J.R., M.D. Fleming, B.F. Molnia, J.H. Dover, J.S. Kelley, M.L. Miller, W.J. Nokelberg, G. Plafker, and A.B. Till, 1997. *Digital Shaded-Relief Image of Alaska*, U.S. Geological Survey Miscellaneous Investigations Map I-2585, scale 1:2,500,000.

Smith, D.E., M.T. Zuber, S.C. Solomon, R.J. Phillips, J.W. Head, J.B. Carvin, W.B. Banerdt, D.O. Muhleman, G.H. Pettengill, G.A. Neumann, F.G. Lemoine, J.B. Abshire, O. Aharonson, C.D. Brown, S.A. Hauck, A.B. Ivanov, P.J. McGovern, H.J. Zwally, and T.C. Duxbury, 1999. The global topography of Mars and implications for surface evolution, *Science*, 284(5419):1495–1503.

Smith, W.H.F., and D.T. Sandwell, 1997. Global sea floor topography from satellite altimetry and ship depth soundings, *Science*, 277(5334):1956–1962.

Thelin, G.P., and R.J. Pike, 1991. *Landforms of the Conterminous United States—A Digital Shaded-Relief Portrayal*, U.S. Geological Survey Miscellaneous Investigations Map I-2206, scale 1:3,500,000.

Tobler, W.R., 1969. An analysis of a digitalized surface, *A Study of the Land Type* (C.M. editor), Final Report on Contract No. DA-31-124-ARO-D-456 to U.S. Army Research Office, Durham, North Carolina, Department of Geography, University of Michigan, Ann Arbor, Michigan, pp. 59–83.

Vigil, J.F., R.J. Pike, and D.G. Howell, 2000. *A Tapestry of Time and Terrain*, U.S. Geological Survey Miscellaneous Investigations Map I-2720, scale 1:3,500,000; http://tapestry.usgs.gov/.

Weibel, R., and M. Heller, 1991. Digital terrain modelling, *Geographical Information Systems—Principles and Applications* (D.J. Maguire, M.F. Goodchild, and D.W. Rhind, editors), Longman, London, U.K., 1:269–297.

Wood, W.F., 1963. *The Relationship of Mask Angles to Terrain Geometry and its Applicability to Military Problems*, Report No. VT-1810-G-2, Cornell Aeronautical Laboratory, Buffalo, N.Y., 40 p.

Yoeli, P., 1967. The mechanisation of analytical hill shading, *Cartographic Journal*, 4(2):82–88.

Yokoyama, R., 2001. Topographical Analysis Maps (a set of maps for all of Japan, including thematic maps of positive openness, negative openness, and slope, and one topographical, all at a scale of 1:500,000), Hokkaido Chizu Co., Asahikawa, Japan.

Yoshikawa, T., S. Kaizuka, and Y. Ota, 1981. *The Landforms of Japan*, University of Tokyo Press, Tokyo, Japan, 222 p. (in Japanese).

Zeitler, P.K., A.S. Meltzer, P.O. Koons, D. Craw, B. Hallet, C.P. Chamberlain, W.S.F. Kidd, S.K. Park, L. Seeber, M. Bishop, and J. Shroder, 2001. Erosion, Himalayan geodynamics, and the geomorphology of metamorphism, *GSA Today*, 11(1):4–9.